OPTICAL INHOMOGENEITIES IN RUBY CRYSTALS

Yu. K. Danileiko, A. A. Manenkov,
A. M. Prokhorov, and V. Ya. Khaimov-Mal'kov

UDC 621.375.82

The optical inhomogeneities in ruby laser crystals, resulting from inhomogeneity of the chromium concentration, from various glide paths, and from the presence of disoriented blocks, are investigated. It is shown that the most harmful influence on the characteristics of laser damage is exerted by the axially asymmetrical part of the refractive index distortion due to residual mechanical stresses. A correlation is obtained between the inhomogeneity of the refractive index and the laser beam divergence. A method is proposed for improving the optical inhomogeneity of the ruby laser crystals by high-temperature (diffusion) annealing.

INTRODUCTION

The optical inhomogeneities that give rise to phase distortions of a light wave passing through a crystal exert a substantial influence on the lasing characteristics of lasers [1]. Among these inhomogeneities the most important are the nonuniformity of the Cr^{3+} concentration, the disoriented blocks, slip tracks, and residual mechanical stresses. The radial inhomogeneity of the distribution of the activator [2-5] has been well studied and is called "chrome lens." It is determined by the structure of the temperature field in the crystal group and usually has axial symmetry. Since the refractive index of ruby increases with the chromium concentration [6] ($dn/df > 0$), whose value increases towards the periphery of the crystal, the active element on the whole is equivalent to a negative lens.

However, such sources of optical inhomogeneity as the residual mechanical stresses, the glide tracks, and the block boundaries are less well studied. The main cause of the appearance of these inhomogeneities in the crystal is apparently the dislocation clusters that form the boundaries of the mosaic block and of the substructure, and also dislocation grids and lattices that form the glide tracks.

The residual mechanical stresses obviously depend on the density and distribution of the dislocations, which can be quite complicated in character.

It should be noted that the dislocation clusters that exist in crystals produce in them not only large-scale (continuous) variation of the refractive index on account of the mechanical stresses, but also small-scale (jumplike) changes. As indicated in [4], such jumps of the refractive index of the crystal can be due to the presence of strong mechanical stress gradients in the region of the glide paths and block boundaries, and also to disorientation of the latter. The discontinuities of the refractive index on the glide paths (over the basal plane) are much stronger for the ordinary ray than for the extraordinary one, whereas in the case of block boundaries the picture is reversed [8]. However, the cause of this dependence of the inhomogeneity of the refractive index on the polarization of the light propagating in the crystal has remained unclear. To explain it, it is necessary to know the dislocation structure of the glide paths and the block boundaries. In the simplest dislocation model of the glide plane one can choose a "horizontal row" of dislocations, i.e., a row such that each dislocation line is made up by the edge of the torn plate terminating on the glide path and perpendicular to it [9].

In this simplest model, the gliding elements over the (0001) plane along the $\langle 11\bar{2}0\rangle$ direction and over the (0001), $(11\bar{2}0)$ planes along the $\langle 1\bar{1}00\rangle$ direction correspond to complete edge dislocations with Burgers vectors along $\langle 11\bar{2}0\rangle$ and $\langle 1\bar{1}00\rangle$, respectively [7] (the planes and directions are designated in accord with the coordinate system shown in Fig. 1).

Translated from Trudy Ordena Lenina Fizicheskogo Instituta im. P. N. Lebedeva, Vol. 101, pp. 130-147, 1978.

 0270-2010/80/0103-0248$07.50

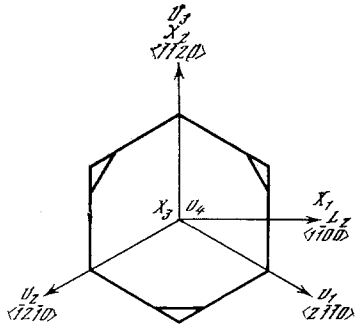

Fig. 1

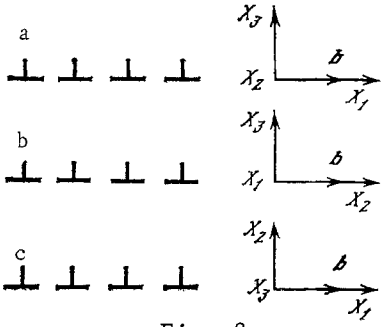

Fig. 2

Fig. 1. Coordinate system used to designate the crystallographic planes and directions. X_1-X_3) Cartesian coordinate system; U_1-U_4) hexagonal coordinate system; L_2) twofold symmetry axis.

Fig. 2. Arrangement of the "horizontal" row of dislocations relative to the chosen coordinate system (see Fig. 1), used to calculate the discontinuity of the refractive index on the glide paths. a) Gliding over the (0001) plane in the ⟨1100⟩ direction (basal gliding); b) gliding over the (0001) plane in the ⟨11$\bar{2}$0⟩ direction (basal gliding); c) gliding over the (11$\bar{2}$0) plane in the ⟨1100⟩ direction (prismatic gliding).

In ruby crystals, gliding along the ⟨1$\bar{1}$00⟩ direction calls for three times more energy consumption than in the ⟨11$\bar{2}$0⟩ direction [10]. It appears that this is the reason why in ruby the glide paths over the basal plane (0001) are the most strongly developed, which are already observed when the crystal is unevenly heated at temperatures of 1300-1400°C [11], and much weaker are glide paths over the prism plane (11$\bar{2}$0), which appear at higher temperatures [12].

The simplest model of a block boundary can be assumed to be a "vertical" row of edge dislocations, the excess planes of which are inclined at an angle θ to the plane at which they terminate. In this case the angle $\theta = b/D$ (b is the Burgers vector of the dislocations and D is the distance between them) is the angle of disorientation between blocks separated by the row of the indicated dislocations [7].

Within the framework of this model the ruby can contain blocks with boundaries produced by dislocations of prismatic glide systems and basal systems. The blocks of the former type have a disorientation axis parallel to the optical axis of the crystal, and consequently are difficult to distinguish by an optical method; the blocks of the latter type, on the contrary, are easily seen when viewed in polarized light [4]. Blocks with a disorientation axis perpendicular to the optical axis can be distinguished also by means of the coefficients of linear expansion. This can lead to the appearance of mechanical stresses on their boundaries when the crystal is cooled after its growth.

The purpose of the present investigations is a more complete clarification of the influence of such crystal lattice defects as glide paths, block boundaries, and residual mechanical stresses on the inhomogeneity of the refractive index. Particular attention is paid to a determination of the main sources of the inhomogeneity of the crystal, which cause an uneven distribution of intensity of the light passing through the crystal in the far zone. Developed methods and apparatus are described for the control of the optical quality and of the residual stresses in ruby crystals. For a quantitative description of the influence of various crystal lattice defects on the inhomogeneity of the refractive index it is necessary to know the piezooptical moduli, which are determined for ruby and corundum crystals below. An analysis of the main source of the optical inhomogeneity has made it possible to develop a special method for reducing the inhomogeneity and for substantially improving the optical quality of ruby laser crystals.

1. INFLUENCE OF GLIDE TRACKS ON THE INHOMOGENEITY OF THE REFRACTIVE INDEX

We analyze now the influence of glide paths on the optical inhomogeneity of ruby crystals. Glide paths can produce considerable amplitude–phase distortions of the light propagating through the crystal only if the light propagation direction lies in the glide plane (or in the block boundary), or else close to it. In this case the light should be strongly diffracted by the discontinuities of the refractive index near the inhomogeneities.

We choose a coordinate system (X_1, X_2, X_3) as shown in Fig. 1, oriented relative to the crystallographic directions in the following manner: the X_1 axis is directed along the $\langle 1\bar{1}00\rangle$ direction (the direction of the twofold axis L_2), the X_2 axis along $\langle 11\bar{2}0\rangle$, and the X_3 axis along $\langle 0001\rangle$ (along the optical axis).

Let the ruby laser element be cut out of the crystal in such a way that the light propagates in it along the axis. In this case one can note in transmitted light inhomogeneities due to gliding over the (0001) plane (basal gliding). If the polarization vector of the light wave is directed along the X_3 axis (e-ray) then the change of the refractive index for this axis due to the mechanical stresses σ_i can be written in the form [13]

$$\Delta n_3^{(2)} \cong -\frac{n_e^3}{2}[\pi_{31}(\sigma_1+\sigma_2)+\pi_{33}\sigma_3], \tag{1}$$

where π_{ij} is the piezooptical tensor. (For the symmetry of this tensor for the group $\bar{3}m$ see, e.g., [13].) For a polarization vector directed along X_2 (o-ray),

$$\Delta n_1^{(2)} \simeq -\frac{n_o^3}{2}[\pi_{11}\sigma_1+\pi_{12}\sigma_2+\pi_{13}\sigma_3+\pi_{14}\sigma_4], \tag{2}$$

where n_o and n_e are the refractive indices of the ordinary and extraordinary rays, respectively. The superscript of the refractive index denotes the light propagation direction. In these formulas we have neglected small rotations of the ellipsoid of the dielectric constant relative to the X_1 axis; this is equivalent to neglecting quantities of second-order smallness relative to Δn_2 and Δn_3.

As seen from Eqs. (1) and (2), shear strains, if at all present on the glide paths, affect the inhomogeneity of the refractive index only for the o-ray.

Let us see that changes are produced in the refractive index by the discontinuity of the normal stresses on glide paths of various types.

1. For basal gliding along the $\langle 1\bar{1}00\rangle$ direction produced by edge dislocations with Burgers vector along $\langle 1\bar{1}00\rangle$ we use the model of "horizontal" row of dislocations [9], arranged as shown in Fig. 2a. The presence in the crystal of such a row of dislocations leads to a discontinuity of the elastic strains on the (X_1X_2) plane, equal to $\Delta U_1 = b/D$. Recognizing, as was done in [9], that the stresses are continuous in the (X_1X_2) plane and that the displacements in the direction of the X_2 axis are equal to zero, we can write:

$$\begin{aligned} \Delta U_1 &= S_{11}\Delta\sigma_1 + S_{12}\Delta\sigma_2 = b/D, \\ \Delta U_2 &= S_{12}\Delta\sigma_1 + S_{22}\Delta\sigma_2 = 0, \end{aligned} \tag{3}$$

where S_{ij} are the components of the compliance tensor, taken from [14]. From (3) we obtain for the discontinuities of the stresses σ_1 and σ_2:

$$\begin{aligned} \Delta\sigma_2 &= \frac{b}{D(S_{12}-S_{11}^2/S_{12})} = 1.43\cdot 10^{12}\frac{b}{D}\left[\frac{\text{dyn}}{\text{cm}^2}\right], \\ \Delta\sigma_1 &= \frac{b}{D(S_{11}-S_{12}^2/S_{11})} = 4.7\cdot 10^{12}\frac{b}{D}\left[\frac{\text{dyn}}{\text{cm}^2}\right]. \end{aligned} \tag{4}$$

2. For basal gliding along the $\langle 11\bar{2}0\rangle$ direction with b along $\langle 11\bar{2}0\rangle$ we have in the approximation of the model of the "horizontal" dislocation row, shown in Fig. 2b,

$$\begin{aligned} &\Delta U_2 = \frac{b}{D}, \quad \Delta U_1 = 0, \quad \Delta\sigma_3 = 0, \\ &\Delta\sigma_2 = \frac{b}{D(S_{11}-S_{12}^2/S_{11})} = 4.7\cdot 10^{12}\frac{b}{D}\left[\frac{\text{dyn}}{\text{cm}^2}\right], \\ &\Delta\sigma_1 = \frac{b}{D(S_{12}-S_{11}^2/S_{12})} = 1.43\cdot 10^{12}\frac{b}{D}\left[\frac{\text{dyn}}{\text{cm}^2}\right]. \end{aligned} \tag{5}$$

Thus, when light propagates in the crystal along the X_2 axis, the dependence of the inhomogeneity of the refractive index on the polarization of the light, as seen from the obtained formulas, can be attributed only to the large difference between the different components of the tensor π_{ij}. Measurements of some of the components of these tensors, which will be described below, yielded the following results [15]:

$$\pi_{11} = 51 \cdot 10^{-7}\,\text{mm}^2 \cdot \text{kgf}^{-1},\ \pi_{33} = 40 \cdot 10^{-7}\,\text{mm}^2 \cdot \text{kgf}^{-1},$$
$$\pi_{12} = -6.8 \cdot 10^{-7}\,\text{mm}^2 \cdot \text{kgf}^{-1},\ \pi_{13} = -9.5 \cdot 10^{-7}\,\text{mm}^2 \cdot \text{kgf}^{-1},$$
$$\pi_{31} = -1.8 \cdot 10^{-7}\,\text{mm}^2 \cdot \text{kgf}^{-1}.$$

Using these data, we obtain for the ratio of the inhomogeneities of the refractive indices of the o and e rays in the case of a glide plane of the first type $\Delta n_1^{(2)}/\Delta n_3^{(2)} = -21.1$. For planes of the second type $\Delta n_1^{(2)}/\Delta n_3^{(2)} = -3.7$.

Consequently, it can be concluded that glide planes over the basis (first type) have the largest anisotropy with respect to the polarization of the incident light.

Similar calculations can be performed for light propagating along the X_1 axis. (The crystal growth axis is parallel to L_2.) In this case $\Delta n_3^{(2)} = \Delta n_3^{(1)}$, and

$$\Delta n^{(1)} \simeq -\frac{n_o^3}{2}(\pi_{12}\sigma_1 + \pi_{11}\sigma_2 + \pi_{13}\sigma_3 - \pi_{14}\sigma_4). \tag{6}$$

In such a propagation of the light in the crystal there will be seen not only glide paths over the basal plane, but also over the prism plane $(11\bar{2}0)$ along the $\langle 1\bar{1}00\rangle$ direction (third type).

Calculation of the discontinuity of the normal stresses in the case of gliding over the prism plane $(11\bar{2}0)$ can be carried out, as was done above, by starting with the model of the "horizontal" row of dislocations with the b vector along $\langle 1\bar{1}00\rangle$ (Fig. 2c). In this case we obtain

$$\Delta U_1 = \frac{b}{D}, \quad \Delta U_3 = 0, \quad \Delta\sigma_2 = 0,$$
$$\Delta\sigma_3 = \frac{b}{D(S_{13} - S_{11}S_{23}/S_{13})} = 0.725 \cdot 10^{12}\frac{b}{D}\left[\frac{\text{dyn}}{\text{cm}^2}\right], \tag{7}$$
$$\Delta\sigma_1 = \frac{b}{D(S_{11} - S_{13}^2/S_{33})} = 4.37 \cdot 10^{12}\frac{b}{D}\left[\frac{\text{dyn}}{\text{cm}^2}\right].$$

Finally, for the glide planes of the first type we have $\Delta n_2^{(1)}/\Delta n_3^{(1)} = -3.7$, for planes of the second type $\Delta n_2^{(1)}/\Delta n_3^{(1)} = -21.1$, and for planes of the third type, which form a perpendicular grid with glide paths over the basal plane, $\Delta n_2^{(1)}/\Delta n_3^{(1)} = -1.7$.

Thus, in crystals grown along the L_2 axis, the glide paths over the basal plane (of the second type), which are most strongly developed in ruby crystals, will have the largest anisotropy relative to the polarization of the incident light, as was in fact observed in [3, 4, 8].

It should also be noted that $\Delta n_1^{(2)}/\Delta n_2^{(1)} = 0.18$, which indicates a lower sensitivity of the ordinary ray to glide paths over the basal plane in the case of crystals grown perpendicular to the L_2 axis than in the case of parallel growth.

It must be kept in mind that for a more accurate calculation of the inhomogeneity of the refractive index on the glide planes it is necessary to know the coordinate dependence of the stress field, the calculation of which for a crystal with corundum symmetry entails considerable difficulties.

To decrease the inhomogeneity of the refractive index for the ordinary ray, as was proposed in [16], we can use crystals grown in such a way that the propagation direction of the light does not lie in the (0001) plane (i.e., there is no diffraction by the glide paths).

However, as will be shown below, crystal growth in a direction perpendicular to L_2 and c will offer advantages with respect to endurance of the crystals to laser radiation.

2. EFFECT OF BLOCKS AND OF RESIDUAL MECHANICAL STRESSES ON THE INHOMOGENEITY OF THE REFRACTIVE INDEX

We now analyze the influence of blocks and residual mechanical stresses in ruby crystals on the inhomogeneity of the refractive index as a function of the polarization of the light and its propagation direction relative to the crystallographic axes.

As shown in [17], in ruby crystals there are two types of blocks: large, elongated along the growth axis, with a large disorientation angle (up to 4°), and small, fan-shaped (mosaic blocks), with center on the boundary of the large blocks which they make up. Let the light in the crystal propagate along the $\langle 1\bar{1}00\rangle$ direction (the crystal was grown along the L_2 axis). In this case if the mosaic block boundaries that make up the large block are made up by a "vertical" lattice of basal gliding edge dislocations with a Burgers vector along X_1, the optical axis of the macroblock will become twisted relative to the X_2 axis [7]. In the entire volume of the crystal (in the absence of macrostresses) one can obtain a linearly polarized wave, which in the case of the e-ray is subject to strong phase distortions. There are two causes of these distortions, which are produced by disorientation of neighboring macroblocks, namely, diffraction by those sections of their boundaries which are parallel to the light propagation direction, and the presence of transverse gradients of the optical path length on account of the differences in the dimensions of the macroblocks along the ray propagation over the cross section of the crystal. In this case two neighboring blocks, disoriented by an angle θ, will differ in their refractive index for the extraordinary ray by an amount

$$\Delta n^e = \theta^2/2\,[(n_e/n_0)^2 - 1]. \tag{8}$$

In the case of the o-ray, the presence of disoriented macroblocks in the crystal can lead to the appearance of amplitude–phase distortions of the wave front only on account of diffraction by those sections of their boundaries which are parallel to the light propagation direction. Such a diffraction can take place only in the presence of a discontinuity of the mechanical stresses on the block boundary. For its calculation it is necessary to know the structure of the boundaries of the macroblocks and the distribution, near them, of the mechanical stress produced when the crystal is cooled, on account of the difference between the expansion coefficient of the corundum along (α_3) and perpendicular (α_1) to the optical axis. An approximate estimate of the discontinuity of the normal stresses for blocks with disorientation axis parallel to X_2 yields a value

$$\Delta\sigma_1 = -\Delta\sigma_3 = \frac{\theta^2\Delta T\,(\alpha_3-\alpha_1)\,(S_{13}+S_{11})}{S_{13}^2 - S_{11}S_{33}}. \tag{9}$$

This formula was obtained from the expression for the ellipsoid of the temperature strains [12] and from an equation of the type (3).

At $\theta = 3\cdot10^{-2}$ rad and at the temperature $T \simeq 1000$°C at which the crystal is cooled we have $\Delta\sigma_3 = 2\cdot10^7$ dyn/cm^2, which yields for the o-ray a refractive index discontinuity

$$|\Delta n_2^{(1)}| \simeq \frac{n_0^3}{2}(\pi_{11}-\pi_{13})\,|\Delta\sigma_1| \simeq 3\cdot10^{-6}.$$

This value of $\Delta n_3^{(1)}$ is too small to cause a noticeable diffraction. A complete calculation of Δn_2 on the block boundary is impossible, since the structure of the boundary is unknown. It can be stated that in weakly stressed crystals the value of Δn_2 is small, as follows from [3, 4, 8].

We now consider the case when the boundaries of the blocks of the mosaic are made up by a "vertical" row of dislocations of basal glide system with a Burgers vector along X_2 ($\langle 11\bar{2}0\rangle$). Such a structure of the boundaries of the mosaic blocks that make up the macroblock causes a twisting of the axis of the latter around the X_2 axis, the latter coinciding with the propagation direction of the light [7]. In this case it is impossible to obtain linearly polarized light in the entire volume of the crystal even in the absence of macrostresses, i.e., an inhomogeneity is produced and causes distortion of the birefringence picture.

In a crystal with such a structure, the inhomogeneity of the refractive index for the e-ray due to the disorientation of the blocks and their different lengths along the light propagation direction will be substantially less than in the case of the block structure described above.

As to the distortions of the wave front of the light passing through the crystal due to diffraction by the boundaries of the macroblocks, their values can likewise not be calculated, since the structure of the block boundaries is unknown.

Estimates of the discontinuity of the mechanical stresses $\Delta\sigma$ due to the cooling of the crystal and to the presence of disoriented blocks can be obtained by the same method as used in the derivation of (9). If the block disorientation axis is parallel to the axis, then

$$\Delta\sigma_3 = [\Delta T\theta(\alpha_3 - \alpha_1)(\theta - 2\varphi)]/S_{33}, \tag{10}$$

where θ is the angle of disorientation of the neighboring blocks; Φ is the angle between the boundary of the blocks and the optical axis of one of them. As seen from (10), this value of $\Delta\sigma_3$ cannot cause noticeable diffraction at disorientation block angles $\theta \simeq 3\cdot10^{-2}$ rad and at $\Delta T \simeq 1000°C$.

We consider now the case when the light propagation direction in the crystal coincides with the $\langle 11\bar{2}0\rangle$ direction (the crystal is grown perpendicular to L_2). In this case, if the mosaic block boundaries are made up by a "vertical" lattice of edge dislocations with a Burgers vector along X_1, the optical axis of the macroblocks will be twisted around the propagation direction of the light. On the other hand if the Burgers vector of the dislocations in the mosaic block boundary is directed along X_2, then the twisting will be around an axis perpendicular to the light propagation direction [7].

Thus, from the considerations advanced above and from the fact that the energy needed to produce in the basal plane dislocations with a Brugers vector along $\langle 11\bar{2}0\rangle$ [7] is one-third as large as in the case of $\langle 1\bar{1}00\rangle$ [13], crystals grown around $\langle 11\bar{2}0\rangle$ should have a smaller optical inhomogeneity for the ordinary ray than crystals grown along $\langle 1\bar{1}00\rangle$.

However, taking into account the entire complexity of the crystal growth process when the Verneuil method is used, the last conclusion calls for a detailed experimental verification. To check on its validity it is necessary to analyze a large amount of statistical data on crystals grown in different directions under most closely identical conditions. No such data are available at present.

We now consider the influence of the residual mechanical macrostresses, produced by the interaction of all the structural defects in the volume of the crystal, on the inhomogeneity of the refractive index. The magnitude of these stresses depends on the dislocation density in the crystal and on the dislocation distribution over its volume. The character of this distribution is determined mainly by the gradient structure of the temperature field during the crystal growth; this structure in most cases has axial symmetry. However, the distortions of the phase front of the light passing through the crystal have no such symmetry. The reason is that the ruby crystals are anisotropic with respect to the linear expansion coefficient α_i, to the compliance moduli S_{ij}, and to the piezooptical moduli π_{ij}. We note that in the presence of a strongly developed block structure in the crystal the symmetry of the field of the residual stresses can also be strongly distorted.

We consider now the refractive index inhomogeneity that can be produced by residual mechanical stresses in a crystal that has a weakly developed block structure, but are produced in an axially symmetric temperature field. By solving this problem we can estimate the residual stresses in the crystal and the radial gradients in the growth oven from the character of the optical inhomogeneity of the grown crystals. Since the exact solution of the problem of the elastoplastic deformation is extremely complicated and calls for knowledge of the characteristics of the anisotropy of the plasticity of the crystal and of its dependence on the temperature, we shall make a number of simplifying assumptions, which make it possible to obtain simple analytic expressions with accuracy sufficient for practical purposes. We shall assume that, first, there is no plasticity anisotropy in the crystal; second, that the plastic deformation in the crystal stops at a certain distance L from the crystallization zone and that this level corresponds to a temperature T_m (L depends on the radial gradients in the oven); third, the residual stresses in the crystal are distributed parabolically in the radial direction (the actual distribution of the stresses is close to this law [18]), which corresponds to a linear growth of the radial temperature gradients; fourth, we can neglect the anisotropy of the compliance moduli S_{ij}, which is not very large for the ruby crystal [19]; the crystal has the form of a long thin cylinder.

Under the foregoing assumptions, we can write for the stress tensor components the expressions [19]:

$$\begin{aligned}\sigma_r &= (\sigma_r)_{\max}(r^2 - 1),\\ \sigma_\theta &= (\sigma_r)_{\max}(3r^2 - 1),\\ \sigma_z &= 2(\sigma_r)_{\max}(2r^2 - 1),\ r = R/R_0,\end{aligned} \tag{11}$$

where R is the radial coordinate; R_0 is the radius of the cylinder; $(\sigma_r)_{max}$ is the maximum radial stress in the crystal.

We note that the law governing the distribution of the stresses (11) corresponds to a linearly decreasing temperature gradient λ_r such that

$$(\sigma_r)_{\max} \simeq \frac{\tilde{\alpha}\lambda}{8(\tilde{S}_{11} + \tilde{S}_{12})}, \tag{12}$$

where

$$\tilde{\alpha} = \frac{\alpha_3 + \alpha_1}{2}; \quad \tilde{S}_{11} = \frac{S_{11} + S_{33}}{2};$$

$$\tilde{S}_{12} = \frac{S_{12} + S_{13}}{2}.$$

For a crystal grown, e.g., along L_2 (twofold symmetry axis), we obtain for the inhomogeneities of the refractive indices of the ordinary and extraordinary rays the respective expressions (see (1) and (2)):

$$\begin{aligned}\Delta n_o &\simeq -\frac{n_o^3}{2}(\pi_{12}\sigma_1 + \pi_{11}\sigma_2 + \pi_{13}\sigma_3),\\ \Delta n_e &\simeq -\frac{n_e^3}{2}[\pi_{31}(\sigma_1 + \sigma_2) + \pi_{33}\sigma_3],\end{aligned} \tag{13}$$

where

$$\begin{aligned}\sigma_1 &= 2(\sigma_r)_{\max}(2r^2 - 1);\\ \sigma_2 &= (\sigma_r)_{\max}[r^2(\sin^2\theta + 3\cos^2\theta) - 1];\\ \sigma_3 &= (\sigma_r)_{\max}[r^2(3\sin^2\theta + \cos^2\theta) - 1]\end{aligned}$$

(θ is the polar angle measured from the optical axis of the crystal).

In (13) we have neglected the rotation of the ellipsoid of the refractive index as a result of the shear strains, since the changes they produce in the refractive index are of second-order smallness in the stresses.

The interference pattern in light transmission through the crystal, due to the mechanical stresses of the indicated symmetry, is determined by the expression $l\Delta n = m\lambda_0$, where l is the length along the ray in the crystal; m is the order of the interference, λ_0 is the wavelength of the light source. As seen from the formulas in (13), the pattern takes the form of ellipses corresponding to a positive lens and rotated for the o- and e-rays 90° relative to each other. For the e-ray the ellipses are elongated along the optical axis. This is precisely the behavior of the interference pattern observed earlier [1] (Fig. 3a). We note that the ratio of the semiaxes of the ellipses a/b on the interference pattern depends on the law of the variation of the radial temperature gradient. If $\text{grad } I = -\lambda r^n$, then $a/b = \sqrt{n+2}$ for the e-ray. In the presence of gradients that depend so strongly on r (large ratio a/b), the influence of the anisotropy of the crystal can already come into play; this anisotropy can lead to the appearance of a saddle point in the inhomogeneity of the refractive index [1] (Fig. 3b).

The foregoing analysis of the influence of the mechanical stresses on the inhomogeneity of the refractive index explains the behavior of the interference pattern of the crystal when light of different polarization propagates in it. However, this analysis does not make it possible to estimate the stresses and the temperature gradients, owing to the distorting influence of the "chrome lens."

To estimate the residual stresses in the crystal, we consider the pattern of the anomalous birefringence, since it is not sensitive to the inhomogeneity of the Cr^{3+} concen-

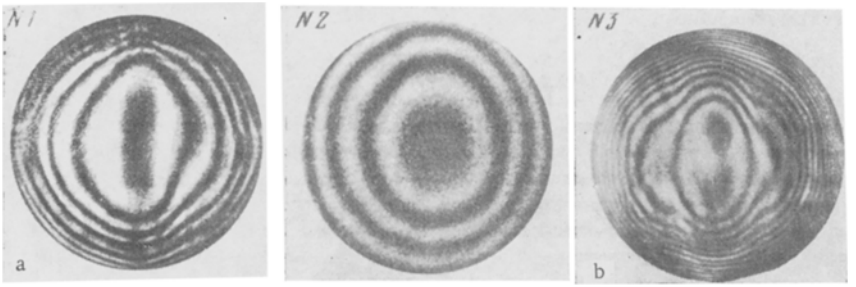

Fig. 3. Interference pattern of a stressed crystal for the e-ray: a) for crystals grown in a temperature field with a weak radial dependence of the temperature gradient (interference pattern of the elliptic type); b) for a crystal grown in a temperature field with a strong radial dependence of the temperature gradient (interference pattern with saddle point).

tration. The character of the pattern of the anomalous birefringence is described by the formula

$$l\,[(n_0 - n_e) + (\Delta n_o - \Delta n_e)] = m\lambda_0, \qquad (14)$$
$$l \simeq l_0\,(1 + \varphi^2/2),$$

where l_0 is the length of the crystal; φ is the angle between the normal to the end surfaces of the crystal and the direction of the wave normal of the light propagating in the crystal ($\varphi \ll 1$) ; m is the order of the interference. Using (13) and the values of the components of the tensor π_{ij}, we can rewrite (14) in the form

$$r^2(\cos 2\theta + 0.16) = \frac{2\cdot 10^5}{n_0^3(\sigma_r)_{\max}}\left[(n_e - n_o) - \frac{m\lambda_0}{l_0(1+\varphi^2/2)}\right], \qquad (15)$$

where $(\sigma_r)_{max}$ is in kgf/mm^2.

As seen from (15), the pattern of the anomalous birefringence in the crystal is a family of second-order curves (hyperbolas). Figures 4a and 4b show the curves calculated from (15) and the experimentally observed birefringence patterns for a ruby crystal with l_0 = 7.5 cm. As seen from Fig. 4, the radial temperature gradient T = λr accounts well for the observed form of the pattern of the anomalous birefringence. There are cases, however, when it takes the form of a curve of higher order than the second (Fig. 4c). This can be due to the stronger radial dependence of the temperature gradient.

Formula (15) presented above makes it possible to estimate $(\sigma_r)_{max}$, while (11) yields all the diagonal components of the strain tensor. This is done experimentally in the following manner: we number the fringes of the anomalous birefringence pattern 1, 2, ..., starting from the center of the crystal along the optical axis. By varying the angle (by inclining the crystal), we cause fringe 1 to pass through the center of the crystal. Then

$$(\sigma_r)_{\max} \simeq 1.8\,\frac{m-1}{l_0}\left(\frac{R_0}{R_{m-1}}\right)^2\left[\frac{\text{kgf}}{\text{mm}^2}\right], \qquad (16)$$

where l_0 is in centimeters; R_{m-1} is the distance between the geometric axis of the crystal and the point of intersection of the m-th fringe with the direction of the optical axis. In (16) the wavelength is λ_0 = 6328 Å. The estimates made for the crystal shown in Fig. 4b yielded for the stresses the following values (in kgf/mm^2): $(\sigma_r)_{max}$ = 0.65; $(\sigma_\theta)_{max}$ = 1.3; $(\sigma_z)_{max}$ = 1.3, corresponding to a radial temperature gradient grad T = − 17r (deg). The use of the described method of estimating the stresses calls for the presence of not less than two fringes in the birefringence pattern (m ⩾ 2), thus limiting the sensitivity of the method ($(\sigma_r)_{\max} > \frac{1.8}{l_0}\left[\frac{\text{kgf}}{\text{mm}^2}\right]$ for a single pass of light through the crystal and $(\sigma_r)_{\max} > \frac{0.9}{l_0}\left[\frac{\text{kgf}}{\text{mm}^2}\right]$ for a double pass).

The presented method of estimating the residual mechanical stresses can be easily generalized to include the case of axially symmetric temperature fields.

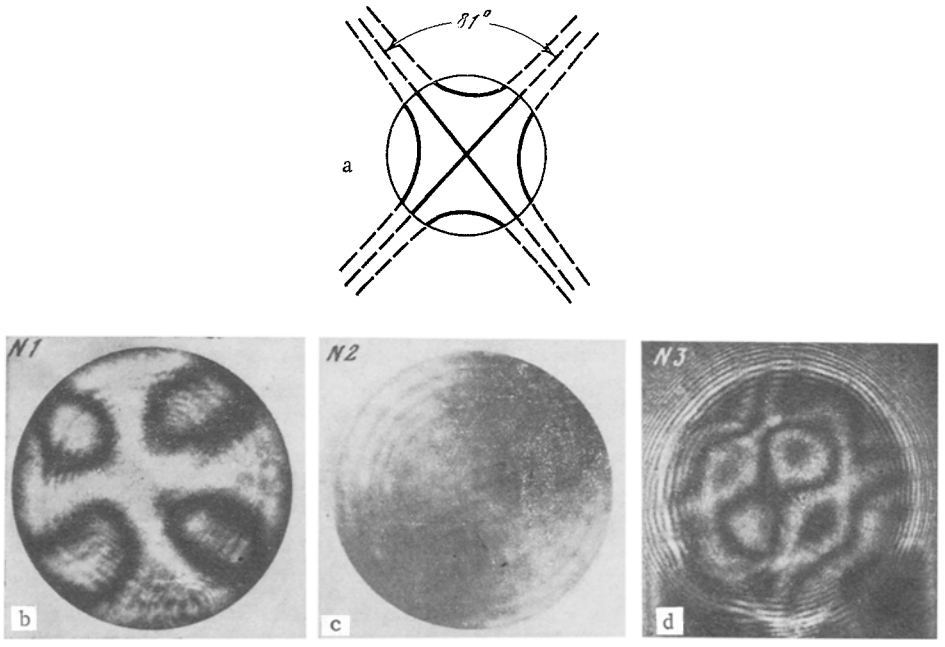

Fig. 4. Pictures of anomalous birefringence of stressed ruby crystal: a) calculated from formula (15); b) for crystals grown in a temperature field with a weak radial temperature gradient; c) for a crystal grown in a temperature field with a strong radial temperature gradient.

The presence of a block structure in the crystal may distort the picture of the anomalous birefringence. These distortions are negligible if the maximum block disorientation angle is $\varphi \lesssim \frac{1}{3}\sqrt{\frac{\lambda_0 n_o}{l_0(n_e - n_o)}}$. For a crystal with l_0 = 7.5 cm we have $\varphi < 2°$.

3. MEASUREMENTS OF THE PHOTOELASTIC MODULI OF CORUNDUM AND RUBY CRYSTALS

In connection with the extensive use of articles made of single-crystal ruby and corundum, it is frequently necessary to know their piezooptical moduli. The published values of the elastooptical moduli of corundum, measured by the dynamic method (plus the adiabatic conditions [20]) can lead to some doubts when used in static problems. Among these problems, e.g., are the estimate of the residual stresses in the crystals after their synthesis and annealing, allowance for the influence of the mechanical stresses on the change of the refractive index, etc. Taking this into account, we measured the piezooptical moduli under isothermally static conditions. We used an interference method, which made it possible to directly calculate these moduli from the dependence of the absolute increment of the refractive index on the stresses applied to the sample, using the formulas [13, 21]

$$\Delta B_{11} = \frac{\Delta n_{13} - \Delta n_{23}}{n_3^3} + \frac{\Delta n_{12} - \Delta n_{32}}{n_2^3} - \frac{\Delta n_{21} + \Delta n_{31}}{n_1^3}, \tag{17}$$

$$\Delta B_{22} = \frac{\Delta n_{23} - \Delta n_{13}}{n_3^3} - \frac{\Delta n_{32} + \Delta n_{12}}{n_2^3} + \frac{\Delta n_{21} - \Delta n_{31}}{n_1^3},$$

$$\Delta B_{33} = -\frac{\Delta n_{13} + \Delta n_{23}}{n_3^3} + \frac{\Delta n_{32} - \Delta n_{12}}{n_2^3} + \frac{\Delta n_{31} - \Delta n_{21}}{n_1^3}, \tag{18}$$

where n_{ij} is the increment of the refractive index along the i direction for polarization in the j direction;

$$\Delta B_{ij} = \pi_{ijkl}\sigma_{kl}.$$

The measurements were made on samples in the form of a parallelepiped with crystallographic faces {0001}, {10$\bar{1}$0} and {11$\bar{2}$0}. In this case the piezooptical moduli π_{ik}, the

normal stresses σ_i, and the absolute increments of the refractive index Δn_{ij} are connected by the relations

$$\pi_{11}\sigma_1 = -2\Delta n_{31}/n_1^3, \quad (19)$$

$$\pi_{11}\sigma_2 = -2\Delta n_{32}/n_2^3, \quad (20)$$

$$\pi_{12}\sigma_2 = -2\Delta n_{32}/n_2^3, \quad (21)$$

$$\pi_{12}\sigma_2 = -2\Delta n_{31}/n_1^3, \quad (22)$$

$$\pi_{33}\sigma_3 = -2\Delta n_{23}/n_3^3, \quad (23)$$

$$\pi_{31}\sigma_1 = 2\Delta n_{23}/n_3^3, \quad (24)$$

$$\pi_{31}\sigma_2 = 2\,[\Delta n_{32} - \Delta n_{12}/n_2^3 - \Delta n_{13}/n_3^3], \quad (25)$$

$$\pi_{13}\sigma_3 = -2\Delta n_{12}/n_2^3, \quad (26)$$

where $n_1 = n_2 = 1.758$; $n_3 = 1.766$.

Measurement Procedure. We investigated leucosapphire and ruby (Cr $\sim$ 0.03%) samples grown by the Stockbarger and Verneuil methods, respectively, and annealed beforehand; their dimensions were 5.5 × 5.8 × 17.35 and 4.78 × 4.78 × 14.8 (face-orientation accuracy $\sim$20, flatness of faces not worse than $\lambda/4$, and their parallelism 2-3"). After adjusting the sample in accordance with the ray reflected from the front face, a small optical wedge was produced, as a result of which interference fringes arranged perpendicular to the long edge of the sample were observed on the screen. The large field of view of the instrument on the screen has made it possible to observe interference fringes both from light beams passing through the crystal (past the sample) and those passing inside the sample (the interferometer field). The latter were used as a reference.

The homogeneity of the stresses in the central part of the sample ($\sim^1/_3$ of the length) was the result of its geometric shape (long parallelepiped), of the uniform load on the sample, as well as of the redistribution of the stress field within narrow limits, effected by displacing the loading device relative to the piston rod of the hydraulic press.

The homogeneity of the stresses was monitored against the bending of the interference fringes of the crystal field relative to the reference fringes of the interferometer field. In the central part of the crystal this distortion did not exceed 0.1-0.15 fringe. Investigations have shown that it is impossible to attain in samples with blocks the uniform stress distribution with the accuracy of which the procedure is capable. The measurements were therefore performed on samples in which there were no blocks (the presence of blocks was monitored by the well known polarization and shadow methods [12, 22]). The load was applied to the investigated samples by a hydraulic press; the error in the measurements of the pressures on the sample did not exceed ±2%. Calculations of the absolute increments of the refractive index Δn for a sample of thickness l at a given pressure were made in accordance with the formula

$$\Delta n = (\pm N_1 - N_2)\,\lambda/2l,$$

where λ is the wavelength of the light source, equal to 6328 Å; N_1 is the number of fringes passing on the screen through the zone of the uniform stresses in the sample (the number of fringes was counted relative to the reference fringe of the interferometer field); N_2 is a correction equal to the change in the number of fringes on account of the geometric increase of the optical path in the crystal. To calculate N_2 we used the elastic compliances S_{12} and S_{13}, equal respectively to -0.0716 and $-0.0364\cdot10^{-12}$ cm²/dyn [20]. The sign of Δn — the sign of $(\pm N_1 - N_2)$ was determined by comparing the direction of motion of the fringes in the course of loading with the direction of their motion when the mirror was translationally displaced.

The measurements were made at a temperature 21°C. An estimate of the change of the sample temperature on account of its deformation under loads on the order of 100 kgf/mm² shows that the change is $\sim10^{-3}$ deg, and the characteristic time of establishment of the temperature field in the sample $\tau_{char} \simeq h^2\varkappa^{-1}$ (h is the maximum sample dimension; $\varkappa$ is the coefficient of thermal diffusivity of ruby) was $\sim$15 sec.

Measurement Results. Figure 5 shows the experimental plots of $2\Delta n_{ij}/n_j^3$ against the stresses σ_i for leucosapphire and ruby samples, and also the calculated dependence of

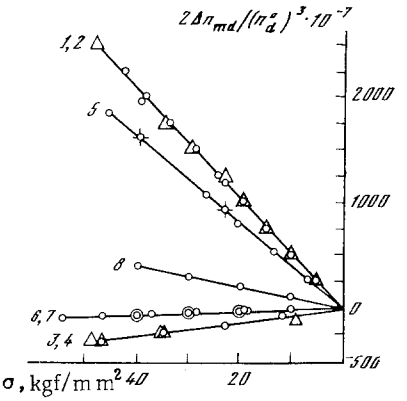

Fig. 5. Dependence of the change of the refractive index $2\Delta n_{ij}/(n_j^3)$ on the stresses τ_i: 1) from (19); 2) from (20); 3) from (21) and (22); 4) from (23); 5) from (24); 6) from (25); 7) from (26); 8) from (27).

$2[(\Delta n_{32} - \Delta n_{12})/n_2^3 - \Delta n_{13}/n_3^3]$ on the stress σ_2. A comparison of the experimental dependences with the calculated one shows not only that they are in satisfactory agreement, but serves also as a check on the obtained experimental values.

The piezooptical moduli calculated from the measurement data turned out to be

$$\pi_{11} = (51 \cdot 10^{-7} \pm 2\%)\ \text{kgf}^{-1} \cdot \text{mm}^2,$$
$$\pi_{33} = (40 \cdot 10^{-7} \pm 2\%)\ \text{kgf}^{-1} \cdot \text{mm}^2,$$
$$\pi_{13} = (-9.5 \cdot 10^{-7} \pm 15\%)\ \text{kgf}^{-1} \cdot \text{mm}^2,$$
$$\pi_{12} = (-6.8 \cdot 10^{-7} \pm 8\%)\ \text{kgf}^{-1} \cdot \text{mm}^2,$$
$$\pi_{31} = (-1.8 \cdot 10^{-7} \pm 25\%)\ \text{kgf}^{-1} \cdot \text{mm}^2.$$

Discussion of Results. It is of interest to note the absence of a difference between the moduli π_{ij} of leucosapphire and ruby (Cr $\sim$ 0.03%) samples made from crystals grown by different methods (the leucosapphire by the Stockbarger method with a dislocation density $\sim 10^3$ cm^{-2}, as revealed by etching on the (0001) plane, and the ruby by the Verneuil method with dislocation density $\sim 10^5$ cm^{-2}).

As already noted above, in the present study we compared the values of the piezooptical moduli determined by dynamic and static methods. A comparison of these values when recalculated in terms of the elastooptical moduli P_{ij} given in [20] ($\pi_{11} = (40.55 + 46P_{14}) \cdot 10^{-7}$ mm^2/kgf, $\pi_{12} = (40.19 + 46P_{14}) \cdot 10^{-7}$ mm^2/kgf, $\pi_{33} = 53.56$ mm^2/kgf, $\pi_{31} = -8.98 \cdot 10^{-7}$ mm^2/kgf, $\pi_{13} = -10.1 \cdot 10^{-7}$ mm^2/kgf) shows them to differ greatly. The reason for this difference remains unclear. It may be due to the stronger sensitivity of the dynamic method to the block structure of the sample. The difference between the measured elastic compliances [14, 23], which are used in the determination of the moduli π_{ij}, likewise does not explain the observed discrepancy.

Another discrepancy with the published data is the disparity in the values of the difference $\pi_{11} - \pi_{12}$. This difference was found by us to be $0.59 \cdot 10^{-7}$ mm^2/kgf as against $0.36 \cdot 10^{-7}$ mm^2/kgf obtained from dynamic measurements [20], and against $0.76 \cdot 10^{-7}$ mm^2/kgf obtained from the dependence of the change of the birefringence on the stresses [18]. Since the quantity $\pi_{11} - \pi_{12}$ is used in many procedures for estimating residual stresses in corundum crystals (see, e.g., [7]), such a disparity is most significant. In our opinion this disparity (the last-mentioned method is static) could be due also to the procedure used to obtain uniform stresses in the measurements, and might be connected with the quality (block structure) of the employed sample.

4. METHOD AND APPARATUS FOR THE MONITORING OF OPTICAL INHOMOGENEITIES IN RUBY CRYSTALS

Ruby crystals grown by the Verneuil method have considerable optical inhomogeneity. The sources of this inhomogeneity are: the inhomogeneity of the chromium concentration, the presence of glide paths and block structure, residual mechanical stresses due to the presence of a complicated dislocation structure of the crystal.*

At the present time there are various methods of measuring the indicated inhomogeneities. The interference method permits a study of the refractive index inhomogeneities due to the presence of the "chrome lens" and to the residual mechanical stresses. One usually uses a Michelson interferometer with mercury or cadmium lamps as the light source [25]. The interference method produces in fact the picture of the phase distortions of the light wave passing through the crystal in the near zone.

The presence of small-scale phase distortions leads in the far zone to a complex diffraction pattern, which is sometimes called small-angle scattering in the literature.

The well-known instrument POKK-1, intended for the investigation of a light wave passing through the crystal in the far zone, yields only the integrated characteristic of the divergence, but does not yield any information on the structure of the distribution of the energy in the far zone.

To investigate local inhomogeneities of the refractive index with strong gradients (glide plane, block boundaries) one uses also instruments with small diaphragms [26], which make it possible to investigate the shadow pattern of crystals (i.e., the amplitude distortions in the near zone of the end face of the crystal).

The residual mechanical stresses are presently measured by using various conoscopes [12, 18, 26]. The stresses in instruments of this type are estimated either from the value of the angle between the optical axes of the crystal, which becomes biaxial in the presence of mechanical stresses, or from the anomalous birefringence.

A shortcoming of the existing methods of estimating the stresses is that the crystal must be viewed along the direction of the optical axis, which usually does not coincide with the geometrical axis of the sample. This method of viewing calls for the use of an immersion liquid.

We have constructed an instrument for the investigation of the optical homogeneity of ruby laser crystals. The principal characteristics of the optical inhomogeneities that cause phase distortions of a light wave passing through the crystal can be obtained with this instrument from the interference pattern, from the anomalous birefringence and also from the distribution of the optical radiation passing through the crystal in the far zone. In addition, using the results of the analysis presented above, it is possible to determine the residual stresses in 90° ruby crystals by measuring the anomalous birefringence.

The schematic diagram of the instrument is shown in Fig. 6 [2]. The light source is a type OKG-11 helium–neon laser operating in the regime of a single longitudinal mode. The lasing was not single-mode with respect to the transverse indices. This operating regime of the laser produces radiation with great time coherence, so that it is possible to use interferometers with large differences between the optical paths. However, the multimode character of the lasing with respect to the transverse indices does not make it possible to use the laser beam directly to investigate the optical homogeneity of the crystals, since the laser has no spatial coherence, as a broad directivity pattern, and its intensity is not uniform over the cross section. To obtain the necessary spatially coherent light field with flat phase and uniform intensity we used a diffraction filter consisting of two confocal lenses and a diaphragm in the region of their focus. The dimension of the diaphragm is determined in such a way that it is somewhat smaller than the diameter of the caustic of the TEM_{00} mode passing through the entry lens in its minimum cross section. A diaphragm of diameter $(4\text{-}6)\cdot10^{-4}$ cm and a lens with focal length $F_1 = 0.8$ cm were used. The focal length of the exit lens was $F_2 = 10$ cm. Such a filter ensured a flat wavefront with accuracy of approximately $\lambda/5$ over a diameter 1.5 cm. This flatness was limited by the dimensions and

*We do not touch here upon methods of investigating dislocations in crystals. They are described, e.g., in [7, 10, 24].

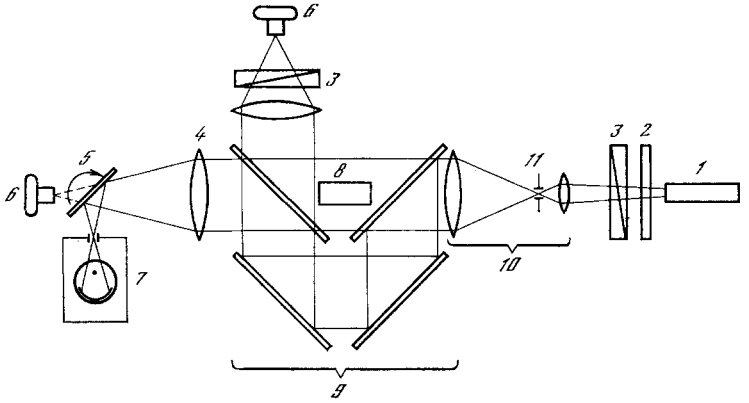

Fig. 6. Schematic diagram of instrument for the monitoring of the optical quality of ruby laser crystals: 1) He–Ne laser; 2) quarter-wave plate; 3) polaroids; 4) long-focus lens (F = 100 cm); 5) tilting mirror; 6) photographic cameras; 7) photomultiplier with slit diaphragm; 8) investigated crystals; 9) Mach–Zehnder interferometer; 10) diffraction filter with round diaphragm 11.

quality of the diaphragm, and also by the spherical aberrations of the exit lens. We note that the advantages of such a filter over an ordinary telescope are that it makes it possible: 1) to dispose of the weak small-scale inhomogeneities, which take place in the radiation of even a single-mode laser, something that cannot be done by telescope; 2) to realize a more compact (in length) system at a given planarity of the wave front on a given diameter than in the case of a telescope, at not too great a loss of intensity. The latter is due to the fact that the divergence of the radiation past the diaphragm is determined not by the focal length of the entry lens, but by the diffraction by the diaphragm. After passing through the investigated crystal, the plane wave shaped by the filter underwent amplitude–phase distortions due to the optical inhomogeneity of the crystal. These distortions in the near zone were revealed by the shadow and interference patterns using a Mach–Zehnder interferometer with a shutter in the comparison arm.

To investigate crystals in polarized light with arbitrary direction of the polarization plane, the radiation from the laser passed through a quarter-wave plate and two rotatable polaroids, between which the investigated sample was placed.

In the far zone, the phase distortions of the wave front of the radiation passing through the filter were observed with a long-focus lens (F = 100 cm), in whose focus was placed either a photographic plate or a slit diaphragm with a photomultiplier. In the latter case the light beam was periodically swept on the slit with the aid of a tilting mirror, so that the divergence of the light beam (the field in the far zone) could be measured directly on the oscilloscope screen. The angular resolution of the apparatus was in this case not worse than 30". The use of a slit diaphragm as the scanning element is justified by the fact that for most ruby crystals the light beam passing through the crystal has a directivity pattern elongated in one direction.

The described instrument could be operated in several regimes.

1. Investigation of phase distortion of the light wave passing through the crystal: The phase distortions were analyzed in the near zone with an interferometer and in the far zone by scanning the light beam passing through the crystal through a slit in the focus of the lens. The investigation can be carried out at arbitrary mutual orientations of the incident light polarization plane, crystal optical axis, and scanning direction.

2. Operation with a small diaphragm is carried out with the shutter in the comparison arm of the interferometer closed, and makes it possible to investigate the shadow pattern of the crystal in both a parallel and diverging light beam. The divergence angle is regulated by moving the exit lens of the diffraction filter.

3. The conoscope regime is realized with the shutter in the comparison arm closed and with the polaroids crossed, and makes it possible to investigate, in the case of a parallel

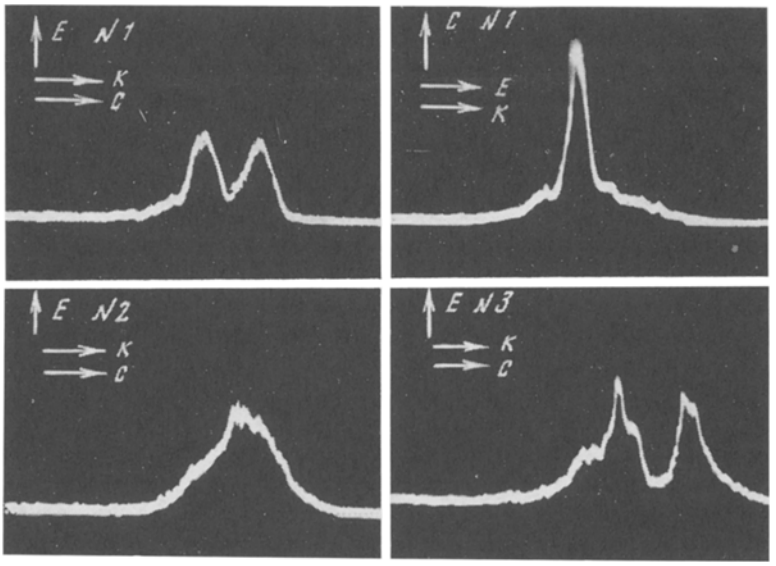

Fig. 7. Oscillogram of the distribution of the energy of optical radiation passing through the crystal in the far zone. E) Electric vector of light wave; C) optical axis of the crystal; K) scanning direction.

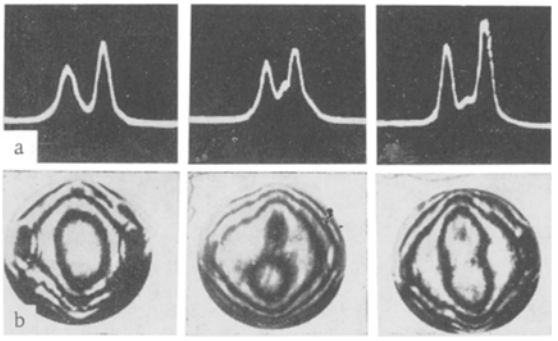

Fig. 8. Interference pattern for o-ray (a) and distribution of energy of the radiation passing through the crystal in the far zone (b) for three ruby crystal samples.

beam, the pattern of the anomalous birefringence, and in the case of a converging beam the conoscopic pattern of the crystal.

5. EFFECT OF CRYSTAL INHOMOGENEITY ON THE DIVERGENCE OF OPTICAL RADIATION PASSING THROUGH IT

The setup described above was used to investigate ruby crystals 75 mm in length grown by the Verneuil method. The chromium concentration of the samples was $\sim$0.03% by weight. The main purpose of the investigation was to determine the causes of the nonuniformity of the energy distribution of the light wave passing through the crystal in the far zone. To this end we compared the interference pattern, the field in the near zone (the shadow pattern), the field in the far zone (the spatial distribution of the light intensity at the focus of the lens), as well as the pattern of the anomalous birefringences.

The picture of the energy distribution in a certain plane Σ_0 (k is the direction of propagation of the light) in the far zone is determined by the amplitude–phase distortions of the light wave when it passes through the crystal, and can be obtained from the distribution of the field in the near zone by using the formula [27]

$$E(xyz_0) = \frac{ike^{i(\omega t - kr_0)}}{2\pi r_0} \int_{\Sigma_0} E(\xi\eta) e^{ik\frac{x\xi+y\eta}{r_0}} d\xi d\eta, \quad (27)$$

where (xyz_0) is the coordinate of the far-zone point on that crystal end face over which the integration is carried out. The field $E(\xi\eta)$ can be easily obtained from the form of the interference pattern. However, since there is no one-to-one correspondence between the fields $E(\xi\eta)$ and $E(xyz_0)$ given by (27), a study of the distribution of the field in the far zone calls for simultaneous observation in the near zone, in order to adequately determine the causes of the field distortion in the far zone.

An investigation [16] of a light wave passing through a crystal has shown that the distribution of the light intensity at the focus of the lens takes the form of a central spot and lateral "whiskers" due to diffraction by the glide paths and block boundaries. However, the bulk of the energy of the light passing through the crystal is contained in the central spot, i.e., in a first-order approximation the influence of these defects (glide paths and block boundaries) on the divergence can be neglected.

We have investigated the distribution of the radiation energy in this spot using the instrument described above. An oscillogram of the energy distribution is shown in Fig. 7. Obviously, such an uneven character of the field picture in the far zone should correspond to amplitude–phase distortions of the wave front also in the near zone. The radial inhomogeneity of the chromium concentration usually produces an almost spherical wave, which can be corrected with an ordinary lens. The inhomogeneity of the stresses distorts significantly the sphericity of the wave front, and it is usually impossible to obtain by corrective measures a far-zone plane wave in the case of stressed crystals. The corresponding distributions of the energy in the far zone have a clearly pronounced inhomogeneous character (Fig. 7). For the ordinary ray, this inhomogeneity is determined mainly by the macrostresses in the crystal. In the extraordinary ray, the energy distribution in the far zone is influenced, besides by the stresses, also by the presence of disoriented blocks. It should be noted, however, that the presence of a block structure in the crystal, as indicated above, can increase the inhomogeneity of the distribution of the structure defects, meaning also the inhomogeneity of the mechanical stresses. Thus, disoriented blocks can cause indirectly, via the inhomogeneity of the stresses, the appearance of optical inhomogeneity for the ordinary ray.

A comparison of the pictures of the radiation field in the far and near zones shows that to each maximum of the intensity in the focus of the lens there correspond definite regions of the crystal, which do not contribute to the other sections of the field. This indicates that the inhomogeneity of the field in the far zone is due not to diffraction of the light, but to refraction by the refractive index inhomogeneities due to the stresses. For example, in the case of a two-peak directivity pattern, each maximum corresponds to one of the halves of the crystal. Such a symmetry of the optical inhomogeneity is seen also on the interference pattern and on the pattern of the anomalous birefringence (Figs. 7 and 8).

In the case of crystals with a very complicated birefringence pattern (complex stress structure) the field distribution in the far zone has a sharply pronounced inhomogeneous character (Fig. 7).

LITERATURE CITED

1. Yu. K. Danileiko, A. A. Manenkov, A. M. Prokhorov, and V. Ya. Khaimov-Mal'kov, Fiz. Tverd. Tela (Leningrad), 19, 2738 (1968).
2. V. S. Doladugina and E. E. Berezina, Opt. Mekh. Prom., 6, 35 (1964).
3. V. S. Doladugina and E. E. Berezina, Opt. Mekh. Prom., 4, 6 (1965).
4. N. M. Melankholin and N. G. Martynova, Kristallografiya, 10, 214 (1965).
5. G. W. Dueker and J. Q. Atwood, Appl. Opt., 4, 109 (1965).
6. J. A. Mandorino, Am. Mineral., 44, 961 (1959).
7. Methods and Instruments for Ruby-Crystal Quality Control [in Russian], Nauka (1968).
8. A. I. Kolyadin, L. E. Ageeva, and L. P. Tyutikova, Fiz. Tverd. Tela (Leningrad), 8, 3254 (1966).
9. V. L. Indenbom and G. E. Tomilovskii, Dokl. Akad. Nauk SSSR, 115, 723 (1957).
10. M. Z. Kronberg, Acta Metall., 5, 507 (1957).

11. M. Venni and E. Z. McCondless,----------* 2, 979 (1949).
12. M. V. Klassen-Neklyudova, Proc. Crystallogr. Inst. Acad. Sci. USSR, No. 8 (1953).
13. J. F. Nye, Physical Properties of Crystals, Clarendon Press, Oxford (1957).
14. J. B. Wachtman, W. E. Tefft, D. G. Lam, and R. P. Stinchfield, J. Am. Ceram. Soc., 43, 334 (1960).
15. E. M. Akulenok, Yu. K. Danileiko, and V. Ya. Khaimov-Mal'kov, Kristallografiya, 15, 1200 (1970).
16. E. M. Akulenok, Kh. S. Bagdasarov, V. S. Papkov, V. Ya. Khaimov-Mal'kov, Kristallografiya, 12, 286 (1967).
17. N. V. Gliki and A. A. Urusovskaya, Kristallografiya, 10, 650 (1966).
18. V. L. Idenbom and T. E. Tomilovskii,Kristallografiya, 3, 593 (1958).
19. L. D. Landau and E. M. Lifshitz, Theory of Elasticity, Pergamon (1968).
20. R. W. Dixon, J. Appl. Phys., 38, 5149 (1967).
21. V. A. Shamburov, Kristallografiya, 7, 379, 593 (1962).
22. V. S. Doladugina, in: Growth of Crystals, Vol. 3, Consultants Bureau (1962).
23. J. Bhimasenchar, Proc. Nat. Inst. (India), 16, 241 (1950).
24. D. Z. Stephens and D. J. Alford, J. Am. Ceram. Soc., 47, 81 (1964).
25. V. S. Doladugina and E. E. Berezina, in: Crystal Growth [in Russian], Vol. V, 402 (1965).
26. N. M. Melankholin and S. V. Grum-Grzhimailo, Methods of Investigating the Optical Properties of Crystals [in Russian], Izd. Akad. Nauk SSSR (1954).
27. F. A. Korolev, Theoretical Optics [in Russian], Vysshaya Shkola (1966).

*Literature citation missing in Russian original — Publisher.